Probing the electronic structure of pure and doped CeMIn$_5$ (M=Co,Rh,Ir) crystals with nuclear quadrupolar resonance

Ján Rusz,[1,2,*] Peter M. Oppeneer,[1] Nicholas J. Curro,[3] Ricardo R. Urbano,[4] Ben-Li Young,[5] S. Lebègue,[6]
Pascoal G. Pagliuso,[7] Long D. Pham,[3] Eric D. Bauer,[4] John L. Sarrao,[4] and Zachary Fisk[8]

[1]*Department of Physics and Material Science, Uppsala University, Box 530, S-751 21 Uppsala, Sweden*
[2]*Institute of Physics, Academy of Sciences of the Czech Republic, Na Slovance 2, CZ-182 21 Prague, Czech Republic*
[3]*Department of Physics, University of California, Davis, California 95616, USA*
[4]*Condensed Matter and Thermal Physics, Los Alamos National Laboratory, Los Alamos, New Mexico 87545, USA*
[5]*Department of Electrophysics, National Chiao Tung University, Hsinchu 300, Taiwan, Republic of China*
[6]*Laboratoire de Cristallographie et de Modélisation des Matériaux Minéraux et Biologiques, CNRS-Université Henri Poincaré,
UMR 7036, B.P. 239, F-54506 Vandoeuvre-lès-Nancy, France*
[7]*Instituto de Física "Gleb Wataghin", UNICAMP, 13083-970, Campinas-São Paulo, Brazil*
[8]*University of California, Irvine, California 92697-4573, USA*

We report calculations of the electric-field gradients (EFGs) in pure and doped CeMIn$_5$ (M=Co, Rh, and Ir) compounds and compare with experiment. The degree to which the Ce $4f$ electron is localized is treated within various models: the local-density approximation, generalized gradient approximation (GGA), GGA+U, and $4f$-core approaches. We find that there is a correlation between the observed EFG and whether the $4f$ electron participates in the band formation or not. We also find that the EFG evolves linearly with Sn doping in CeRhIn$_5$, suggesting the electronic structure is modified by doping. In contrast, the observed EFG in CeCoIn$_5$ doped with Cd changes little with doping. These results indicate that nuclear quadrupolar resonance is a sensitive probe of electronic structure.

PACS number(s): 71.27.+a, 74.70.Tx, 76.60.Gv, 74.25.Jb

I. INTRODUCTION

Nuclear magnetic resonance (NMR) and nuclear quadrupolar resonance (NQR) provide detailed information about the local spin environment in condensed-matter systems.[1] These techniques are particularly important in the study of f-electron systems and have shed light on diverse aspects of these materials, ranging from the symmetry of the superconducting state of unconventional superconductors to the suitability of different materials for nuclear waste storage.[2,3] For certain nuclei, the interaction between the nuclei quadrupolar moment and the local electric-field gradient (EFG) can provide detailed information about the local *charge* environment. This information can be particularly important in the study of f-electron systems, where the f electrons exhibit a delicate balance between localized and delocalized behaviors. In principle, the EFGs at the nuclear sites in the material can reflect the degree of hybridization of the f electrons. By measuring the quadrupolar interaction at these sites, one, therefore, can shed light on the electronic structure.

In this paper, we show that the EFG at the ligand sites in heavy-fermion systems offers a new window on the electronic structure of these f-electron systems. We focus on the case of the CeMIn$_5$ family (with M=Co, Rh, or Ir, i.e., the Ce-115 compounds). The Ce-115's have received considerable interest in recent years as a model system for heavy-fermion behavior. This class of Ce compounds displays an exceptional richness in low-temperature electronic phenomena, including heavy-fermion behavior and antiferromagnetic fluctuations together with unconventional superconductivity.[4–9] The emerging electronic order parameter depends sensitively on the applied pressure and the mag-

netic field; these features, combined with the availability of high-quality single crystals, make them ideal candidates for fundamental studies of the interplay of magnetism and superconductivity. At ambient pressure CeCoIn$_5$ and CeIrIn$_5$ are heavy-fermion superconductors[10,11] whereas CeRhIn$_5$ is an antiferromagnet with an incommensurate helical spin structure.[11,12] By applying pressure—either hydrostatic or chemical (alloying)—one can tune between antiferromagnetism and superconductivity.[13–15] Recently, systematic chemical substitutions in the Ce-115 lattice has provided new information on the interplay of superconductivity and antiferromagnetism.[16–18] A recent study on Cd-doped CeCoIn$_5$ revealed that in the superconducting phase, there is a quantum critical end point of an antiferromagnetic transition hidden.[16] The sensitivity of these systems to electron or hole doping (by alloying with Cd or Sn) suggests that obtaining information about the role of f electrons in these compounds, in conjunction with chemical substitutions, is a crucial step in understanding their properties.[19]

Theoretical descriptions of f-electron materials are notoriously difficult due to strong electron–electron correlations in the open f-subshells. Standard approximations based on the homogeneous electron-gas approximation, such as the local-density approximation (LDA) or the generalized gradient approximation (GGA), place the partially occupied f band in the vicinity of the Fermi level—describing them as itinerant. By artificially switching off the hybridization of f states with other valence electrons, an opposite limit can be reached, treating the f electrons as localized atomiclike states. By methods such as the LDA+U,[20,21] one can tune the system between these two extreme limits through the value of the Coulomb U.

245124-1

In this work we investigate the Ce-115 systems by means of NQR experiments and first-principles calculations. The EFG, determining the quadrupolar resonance frequency ν_Q, is a sensitive probe of the local electronic structure. We compare measured and computed ν_Q frequencies to investigate the f-electron behavior in these materials. We also perform detailed studies of the trends in evolution of the EFG as a function of doping and pressure compared to simulations within different models for the f electrons, which reveals important information about the f-electron behavior in these systems.

II. EXPERIMENT METHODS

For nuclei with spin $I > \frac{1}{2}$, the quadrupolar moment, Q, couples to the local charge distribution via the electric-quadrupole interaction, with Hamiltonian

$$\mathcal{H} = \frac{eQV_{zz}}{4I(2I-1)}[(3\hat{I}_z^2 - \hat{I}^2) + \eta(\hat{I}_x^2 - \hat{I}_y^2)], \qquad (1)$$

where e is the electron charge, Q is the quadrupolar moment, $V_{\alpha\beta}$ are the components of the EFG tensor, and $\eta = (|V_{xx}| - |V_{yy}|)/|V_{zz}|$ is the asymmetry parameter of the EFG. The NQR frequency (in zero field) is defined as $\nu_Q = \nu_z \sqrt{1 + \eta^2/3}$, where

$$\nu_z = \frac{3eQV_{zz}}{2I(2I-1)h} \qquad (2)$$

and h is Planck's constant. For a site with axial symmetry ($\eta = 0$), there are $2I - 1$ quadrupolar resonances at frequencies $n\nu_Q$, where $n = 1, \ldots, 2I - 1$. If $\eta > 0$, then the resonances are not equally spaced. The EFG is fully characterized by three parameters: ν_z, η, and a unit vector, $\hat{q}$, in the direction of the principle axis of the EFG with the largest eigenvalue.

The interaction in Eq. (1) is significant in the Ce-115's because ^{115}In (95.8% abundance) has nuclear spin $I = 9/2$ and quadrupolar moment $Q = 0.81$ barn. Typically the quadrupolar interaction dominates the NMR spectra and also contributes a significant nuclear Schottky contribution to the specific heat in zero field.[22] Clearly, a detailed understanding of the EFG is crucial for analyzing both NMR and low-temperature calorimetry results.

The Ce-115's crystallize in the tetragonal HoCoGa$_5$ structure in which there are two inequivalent In sites (Fig. 1). The In(1) lies in the center of the basal plane close to four Ce atoms. The high symmetry of this position leads to a vanishing asymmetry parameter and an EFG vector $\hat{q} = \hat{c}$. The In(2) has a fourfold multiplicity and has a lower symmetry with nonzero η, with $\hat{q} = \hat{a}, \hat{b}$ (pointing perpendicular to the face of the unit cell). Because of the lower symmetry, one can assume a larger nonspherical part of the density and potential, i.e., a larger EFG at this position. On the other hand, due to the larger distance from the Ce atoms compared with the In(1)-Ce distance and the fact that only two Ce atoms are nearest neighbors, we expect that the EFG at In(2) will be less sensitive to the details of the electronic density around the Ce atom position.
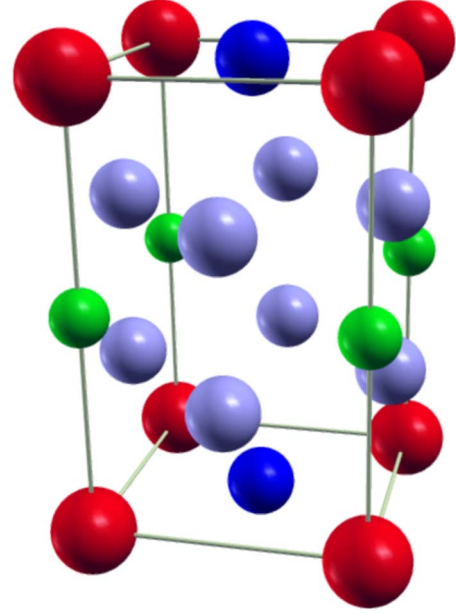

FIG. 1. (Color online) Structure of the CeMIn$_5$ compounds. Red (large) spheres are Ce atoms, green (small) spheres are transition-metal M atoms, and medium sized blue spheres are In atoms. The In(1) (dark blue) with a multiplicity of one is situated in the center of the basal plane and has tetragonal point-group symmetry. In(2) atoms (light blue) with a multiplicity of four have the z component as a free parameter and the lower symmetry of their position leads to nonzero η (see text).

III. COMPUTATIONAL METHODS

We performed first-principles calculations based on the density-functional theory. A state-of-the-art implementation of the full-potential localized augmented planes waves (FPLAPW)–WIEN2K package[23]–was applied, which includes spin-orbit (SO) interaction.[24] It incorporates also the calculation of the EFGs (Ref. 25) using methods described in Refs. 26 and 27.

Our calculations were performed for the Ce-115 materials in the nonmagnetic state, which is an approximation for CeRhIn$_5$ that has a magnetic transition temperature of $T_N = 3.8$ K.[13] CeCoIn$_5$ and CeIrIn$_5$ are nonmagnetic superconductors at low temperatures and ambient pressures.[10,28] We adopted the experimental lattice parameters; the radii of the atomic spheres were 2.5, 2.5, and 2.3 a.u. for Ce, M, and In atoms, respectively (Bohr radius, 1 a.u. = 0.52917 Å). The computational parameter determining the basis size, $RK_{max} = 7.5$, turned out to be sufficient to determine the EFG on In atoms with an accuracy better than 0.5%. The same holds for the Brillouin-zone (BZ) sampling, which we performed with 2000 k points. In our calculations the spin-orbit interaction was normally included while test calculations were performed without SO interaction. We did not add relativistic local orbitals to the scalar-relativistic FPLAPW basis, as this can perturb the EFG value. For exchange and correlation effects we used both the LDA (Ref. 29) and GGA (Ref. 30). We, furthermore, performed relativistic GGA+U calculations[20,21] in which an additional on-site Coulomb interaction for the f-states manifold is introduced. We assumed

here that both the Hubbard U and exchange J parameters do not depend on the m-quantum number of the f states. Consequently, only the effective U value, $U_{eff}=U-J$, enters the calculations.

We have also calculated the doping and pressure dependences of the EFGs. For the doping dependence, it is important to realize that the virtual crystal approximation (VCA)–although it appears as the most suitable tool due to closeness of In with Cd or Sn atoms (denoted as X in the following text)–cannot be applied. The reason is that within the VCA, we work with an effective (averaged) Z (atomic number) at the sublattice where the substitution takes place. This radically influences the electronic density closely around the $In_{1-x}X_x$ sublattices, resulting in nonphysical EFGs. It is important to note that with Cd or Sn doping, the In EFGs are experimentally probed on *other* In atoms than the substituted ones. Consequently, it is vital to keep the core charge of the In atom at these sublattices. Another, straightforward approach, which we pursued here, is to perform supercell calculations. The real doping[16] is at the level of a few atomic percent, which means that rather large supercells are required. Again another approach, which we applied, is based on the observation that the doping results (partially) in adding itinerant electrons or holes to the system. The idea is then to calculate the EFG for a *charged* unit cell, i.e., a unit cell with the same atomic cores as a pure compound yet with an added or subtracted small amount of valence electrons.

IV. RESULTS

Prior to our studies of Ce-115 systems, we investigated the ^{115}In NQR frequency for the parent material $CeIn_3$ of the Ce-115's. Under the assumption of localized Ce f electrons, we obtained an NQR frequency of 9.93 MHz, which is rather close to the experimentally observed value of 9.6 MHz.[31] If we adopt the itinerant description of the Ce f electron, we obtain a somewhat higher value of 10.21 MHz. Our observation that better agreement is achieved for the f-localized approach is consistent with experimental results, which reveal localized behavior of the $4f$ electrons in this system at equilibrium conditions.[32] Furthermore, this agreement provides confidence that our computational approach is applicable to the Ce-115 compounds studied here.

A. Nuclear quadrupolar resonance of pure Ce-115 compounds

The measured ^{115}In quadrupolar resonance frequencies in the three pure compounds are summarized in Table I. These values were determined by fitting the NQR resonances (measured at 4 K) to the Hamiltonian in Eq. (1). To facilitate comparison, we have converted the computed EFGs to quadrupolar frequencies. In the calculations, we have tested the influence of the SO interaction and the choice of the exchange-correlation functional (LDA vs GGA). To investigate the nature of the Ce f electrons, we adopted two extreme situations assuming that the f electrons are either (a) fully localized or (b) itinerant. The localized approach is based on the open-core method treating one Ce f electron as a localized core state and excluding the f subspace for va-

TABLE I. Experimental and theoretical NQR frequencies and asymmetry parameters η in $CeCoIn_5$, $CeRhIn_5$, and $CeIrIn_5$. Values are given in MHz except for η. Results of calculations with spin-orbit interaction included are presented for various LDA and GGA based exchange-correlation potentials. Experimental values are taken from Refs. 33 and 34. Note that $\nu_Q=\nu_z$ if $\eta=0$.

	In(1)	In(2)	
$CeCoIn_5$	ν_z	ν_z	η
LDA itinerant	9.24	16.65	0.300
LDA localized	8.53	16.00	0.363
GGA itinerant	8.89	16.40	0.306
GGA $U=1$ eV	8.76	16.52	0.305
GGA $U=3$ eV	8.20	16.67	0.307
GGA $U=6$ eV	8.03	16.67	0.309
GGA localized	8.24	15.71	0.374
Experimental	8.17	15.49	0.39
	In(1)	In(2)	
$CeRhIn_5$	ν_z	ν_z	η
LDA itinerant	8.27	17.67	0.361
LDA localized	7.09	17.21	0.429
GGA itinerant	7.94	17.30	0.363
GGA $U=1$ eV	7.87	17.38	0.363
GGA $U=3$ eV	7.87	17.33	0.369
GGA $U=6$ eV	8.05	17.00	0.386
GGA localized	6.84	16.81	0.432
Experimental	6.78	16.67	0.45
	In(1)	In(2)	
$CeIrIn_5$	ν_z	ν_z	η
LDA itinerant	7.77	18.91	0.354
LDA localized	5.96	18.71	0.364
GGA itinerant	7.42	18.59	0.358
GGA $U=1$ eV	7.26	18.69	0.359
GGA $U=3$ eV	6.26	18.94	0.369
GGA $U=6$ eV	5.95	18.95	0.372
GGA localized	5.66	18.33	0.367
Experimental	6.07	18.17	0.46

lence states from the Ce atomic sphere. The itinerant LDA or GGA description treats f states as all other valence states. Apart from these, we performed also GGA+U calculations for these compounds for three different effective U values, $U=1$, 3, and 6 eV. A U value of 6 eV is typical for a Ce compound with a high degree of f electron localization (see, e.g., Ref. 35).

The calculated EFGs show only a weak dependence on the selected exchange-correlation potential of the order of 2%–4%, always giving systematically a smaller value within the GGA. The effect of the SO interaction on the EFG is even weaker. On the In(1) position the SO interaction reduces the EFG by approximately 1% and on In(2) the change is below the level of numerical accuracy of the EFG calculation (defined by basis size and BZ sampling as discussed

above). Both the presence of SO interaction and selection of a particular exchange-correlation functional have a negligible influence on the asymmetry parameter η.

Important for our physical discussion is that the difference of ν_z that was predicted for f itinerant and localized models [about 10% and more on In(1)] is well beyond all factors influenced by the accuracy of the EFG determination. Particularly, CeIrIn$_5$ is very sensitive to the selected model for the Ce f states, giving a 23% reduction of ν_z within the localized Ce f model when compared to the itinerant f model. On In(2), this difference is 2%–4%—nearly by an order of magnitude smaller than on the In(1) atom, i.e., it is really the In(1) ligand atom, which is surrounded by four Ce as well as being the closer (ligand) In atom, which is a sensitive probe of the Ce f character. The asymmetry parameter η of In(2) is to some extent also more sensitive to the choice of the f electron model.

The following observations can be made by comparing calculated and experimental ν_z. For CeRhIn$_5$ the f electron is known to be localized, a finding which was concluded from neutron scattering and de Haas–van Alphen experiments.[11,15,36–38] The f-localized description works very well for the NQR frequencies and asymmetry parameter of CeRhIn$_5$. Neither GGA or GGA+U gets close to the experimental values. For CeCoIn$_5$ the situation is more complex. The f itinerant model does not provide a good description. For the In(1) both the GGA+U ($U=3$ eV) and open core (localized f states) compare well to the experiment. The U $=3$ eV calculation is relatively close to the itinerant description of the f states. This observation is consistent with other experimental observations in CeCoIn$_5$, which suggest that not only is this material close to a quantum critical point,[39] but, with temperature, the f electrons exhibit a two-fluid behavior with properties of both localized and itinerant characters.[40,41] A complex situation is also found for CeIrIn$_5$. The f itinerant description appears to overestimate the $\nu_z[\text{In}(1)]$ while the localized description underestimates it. GGA+U goes in the right direction, a U value between 3 and 6 eV gives agreement with experiment for the In(1) position. On the In(2) position, the f localized model would give better agreement with the experimental data but we note that there is no f electron description that explains the asymmetry parameter η. Thus, our calculations indicate less localized f states in CeIrIn$_5$ than in CeRhIn$_5$ but it is more difficult to compare the degree of f electron localization in CeIrIn$_5$ with that in CeCoIn$_5$ from our results. An earlier NQR investigation of CeIrIn$_5$ indicated that the f electrons in this material are more itinerant than, e.g., the heavy-fermion system CeCu$_2$Si$_2$.[4] We also note that differences observed in NQR experiments[42,43] on CeCoIn$_5$ and CeIrIn$_5$ under pressure were interpreted as an indication for more itinerant f electrons in CeIrIn$_5$ than in CeCoIn$_5$. At equilibrium conditions, on the other hand, the lattice parameter of CeCoIn$_5$ is smaller than that of CeIrIn$_5$, which would indicate more hybridization between f and conduction electrons in CeCoIn$_5$.

B. Doped Ce-115's

We have measured the quadrupolar spectra in several doped samples in order to investigate the changes in the
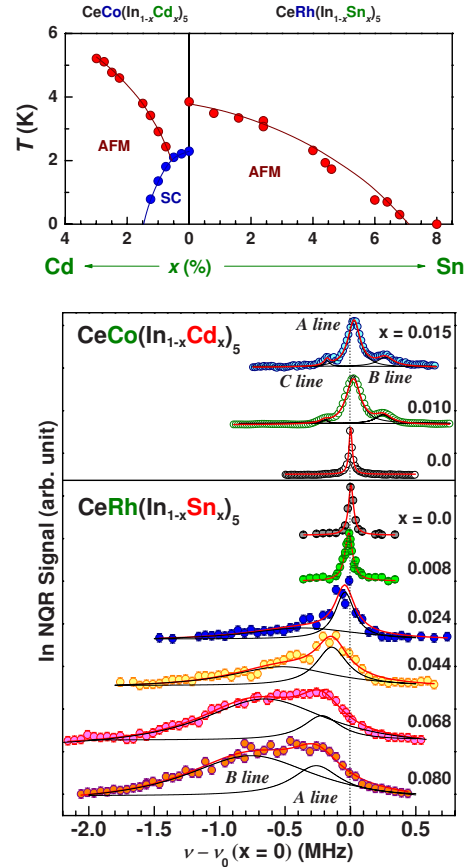

FIG. 2. (Color online) Top: Phase diagrams of CeCo(In$_{1-x}$Cd$_x$)$_5$ and CeRh(In$_{1-x}$Sn$_x$)$_5$ as a function of Cd- and Sn-doping concentration x, respectively. Bottom: Measured NQR spectra of the In(1) $2\nu_Q$ transition $(\pm\frac{3}{2} \leftrightarrow \pm\frac{5}{2})$ in CeCo(In$_{1-x}$Cd$_x$)$_5$ and CeRh(In$_{1-x}$Sn$_x$)$_5$ for the actual concentration x. The x-axis origin has been shifted by the resonance frequency $\nu_0 = \nu_Q(x=0)$. The solid lines are fits, as described in the text.

electronic structure with doping. Figure 2 (top) shows the experimentally determined phase diagrams of CeCo(In$_{1-x}$Cd$_x$)$_5$ and CeRh(In$_{1-x}$Sn$_x$)$_5$ as a function of Cd and Sn dopings x, respectively.[16,17] At the experiment's temperature of 4–5 K, Sn-substituted CeRhIn$_5$ is nonmagnetic while Cd-substituted CeCoIn$_5$ becomes antiferromagnetic for Cd concentrations above 2%. Figure 2 (bottom) shows the experimental NQR spectra of CeRh(In$_{1-x}$Sn$_x$)$_5$ and CeCo(In$_{1-x}$Cd$_x$)$_5$ as a function of doping, and Fig. 3 shows the doping dependence of the resonance frequencies. *A priori*, we expect Sn (Cd) doping to be equivalent to electron (hole) doping since Sn (Cd) lies to the right (left, respectively) of In in the Periodic Table. The change in the electron count in principle can affect the Fermi surface (FS), and hence, the EFG at the In sites. One can understand the doping dependence qualitatively by realizing that a significant portion of the EFG at the In(1) site must arise from the $5p$ electrons of the In. If the $5p$ shell were fully occupied then the EFG should vanish.[44] On the other hand, if the states at the Fermi level have some $5p$ character, there ought to be an on-site contribution to the EFG. As the doping level changes, the character of the states at the Fermi level can change, which in turn can be reflected in the EFGs. Clearly, hole and
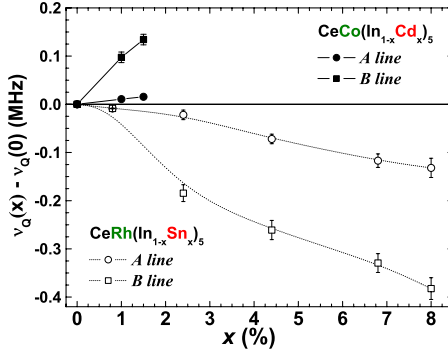
FIG. 3. (Color online) Doping dependence of the NQR resonances measured for $CeCo(In_{1-x}Cd_x)_5$ and $CeRh(In_{1-x}Sn_x)_5$. Dotted and solid lines are guides to the eye. The x values are given in real doping values rather than nominal ones (cf. Ref. 16).

electron dopings have opposite effects on the EFG, and upon doping a second peak appears in the spectra (the B line). This second line is related to In sites proximate to the dopants,[19] as we shall show later on. The relaxation rates, T_1^{-1}, measured at the A and B lines diverge at the bulk Néel temperature, and we conclude that the B line is an intrinsic feature of the doped Ce-115 compounds.[45] The Néel temperature of the C line in Cd-doped $CeCoIn_5$,[16] on the other hand, does not coincide with that of the bulk and may be associated with an impurity phase. We therefore focus only on the EFG at the A and B lines.

We have modeled theoretically the effect of doping. As anticipated, the VCA is unsuitable for the electron or hole doped systems. The reason is that the quadrupolar frequency sensitively depends on the particular atomic nucleus and, within VCA, one works with effective atoms with noninteger core charge. The VCA can, however, be modified to solve this insufficiency. We have, in particular, employed two methods to study the alloying.

1. Modified VCA calculations

The first method is a modification of VCA and permits us to retain the small tetragonal unit cell. The extra (or missing) charge is assumed to be itinerant and only the number of valence states is changed while the core charge is kept. Using this method we can reproduce the experimental trend of the decrease in the main line (A) frequency in $CeRh(In_{1-x}Sn_x)_5$. The results of these LDA calculations are summarized and compared to experiment in Table II. Since the shift in ν_Q is approximately linear with concentration x,

TABLE II. Comparison of experimental and calculated dependences of the NQR frequencies on doping. Given are the frequency shift of the NQR mainline frequency, $[\nu_Q(x) - \nu_Q(x=0)]/x$, in kHz/%. The calculations were performed with both the LDA f-core and f-itinerant approaches.

	f itinerant	f core	Exp.
$CeCo(In_{1-x}Cd_x)_5$	−5.4	5.0	2.1
$CeRh(In_{1-x}Sn_x)_5$	5.4	−14.7	−3.1

we list the slopes, $[\nu_Q(x) - \nu_Q(x=0)]/x$, in Table II. Once again, these results indicate that with the f-core model for $CeRh(In_{1-x}Sn_x)_5$, we can reproduce the trend in agreement with experiment whereas the f-itinerant approach fails. The situation for $CeCo(In_{1-x}Cd_x)_5$ is more complex, as neither the f-core nor the f-itinerant model provides a satisfactory explanation; the trend is better captured by the f-core model. We note that the assumption of extra or missing charge is somewhat simplified in that not all added or removed electrons are free and some of them are expected to stay close to the dopant atom. This is reflected in the predicted trend for both $CeCoIn_5$ and $CeRhIn_5$, which is somewhat too steep, indicating that only a part of the added or removed electrons are free.

Doping was found to have a pronounced influence on the low-temperature properties of Ce-115 materials. In particular, the effect of Cd substitution in $CeCoIn_5$ received attention recently, because it was observed that through Cd doping, $CeCoIn_5$ could be tuned from a superconducting state to an antiferromagnetic state,[16,19,46] which demonstrated the proximity of nonmagnetic $CeCoIn_5$ to magnetic ordering. The origin of the ground-state change and how it emerges locally in the doped lattice are not yet well understood; it was suggested that antiferromagnetism develops locally in the vicinity of the Cd dopants.[19] Also, a relation to an evolvement of the Fermi surface through hole doping was proposed.[19] Our electronic structure calculations for Cd-doped $CeCoIn_5$ can shed light on this issue. We have computed the FS of $CeCo(In_{1-x}Cd_x)_5$ for several doping concentrations, adopting the modified VCA approach. At low temperatures (<500 mK), de Haas–van Alphen experiments[36,47] indicate a substantial degree of f-electron delocalization in $CeCoIn_5$. Therefore we consider here the influence of Cd doping, assuming the f-itinerant approach. Also, the LDA or GGA $4f$-core band structure (see, e.g., Ref. 37) does not display a significant variation in the energy bands in the vicinity of the Fermi level, which implies that for the f-core model, the doping induced changes in the FS are very small. The situation is different for the f-itinerant model where there exist several flat f-related bands close to the Fermi level.[37] In Fig. 4 we show the computed Fermi surfaces of $CeCo(In_{1-x}Cd_x)_5$ for two different doping concentrations, $x=01$ and 0.3. These doping concentrations are relatively large, but they serve to illustrate clearly the trend in the FS evolution. The FSs shown in Fig. 4 can directly be compared to the published results[38] obtained with the f-delocalized approach for $CeCoIn_5$ and the f-localized approach for $CeRhIn_5$ (not shown here). The FS sheets computed for $CeCo(In_{1-x}Cd_x)_5$ with $x=0.1$ are comparable to those of pure $CeCoIn_5$ except for some changes. The FS sheet shown in the top-left panel, which consists of a Γ and an X point centered hole pocket, has expanded, as compared to the pure $CeCoIn_5$, due to the Cd-hole doping. The FS sheet in the middle-left panel, which is electronlike, is quite similar to the corresponding sheet of pure $CeCoIn_5$ except that the cylindrical part with axis along the A-M symmetry line has become a closed cylinder (cf. Ref. 38). The FS sheet in the bottom-left panel has a topology that is different from the corresponding electron sheet in the pure material, where there exists a connected network of tubular shaped arms. Due
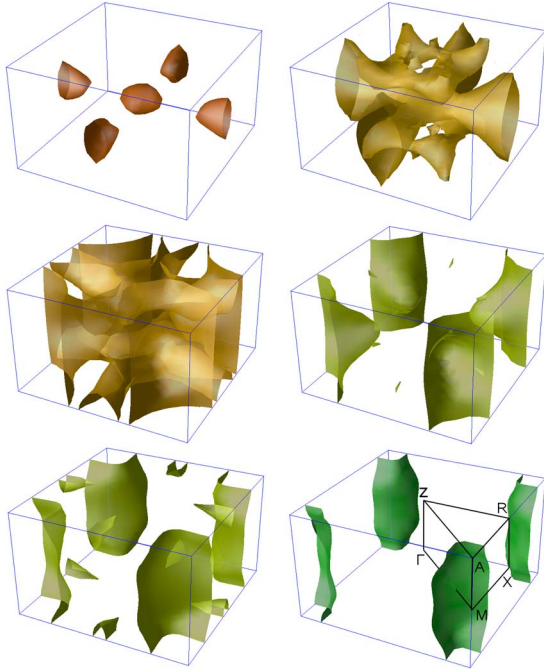
FIG. 4. (Color online) Computed Fermi-surface sheets of CeCo(In$_{1-x}$Cd$_x$)$_5$ for $x=0.1$ (left panels) and $x=0.3$ (right panels). The irreducible Brillouin-zone wedge with high-symmetry points indicated is shown in the lower-right panel.

to the hole doping, the connected network has broken up and only an isolated pocket at the R point remains. This trend of the FS modifications with doping continues when going to higher doping concentrations. The disconnected hole pockets expand further and form a three dimensional network (top-right panel). The complex electron FS in the middle panel shrinks further and only a single cylindrical sheet along the A-M axis remains. A similar change happens for the bottom-right FS sheet, which, in addition, becomes narrower. Altogether, the obtained Fermi surface has now become much more two dimensional than the original FS of the pure material. Importantly, we note that the shape of the FS is now very similar to the $4f$-core FS computed for CeRhIn$_5$ (cf. Ref. 38). Consequently, substitution of Cd in CeCoIn$_5$ leads to typical modifications of the FS, which starts to resemble the FS computed for CeRhIn$_5$ with the f localized approach. The latter material exhibits antiferromagnetic ordering[13] below $T_N \approx 3.8$ K, which is also observed for Cd-doped CeCoIn$_5$ (below $T_N \approx 2-3$ K).[16] This strongly suggests that, in the case where superconductivity and antiferromagnetism are competing order parameters on the FS, the disappearance of superconductivity and the concomitant occurrence of antiferromagnetic order with Cd doping are related to specific modifications of the Fermi surface, which lead to a FS topology that is more favorable for magnetic ordering than for superconductivity.

The doping concentrations of $x=0.1$ and $x=0.3$ are quite large values compared to experimental doping concentrations of a few percent. As mentioned above, the larger doping values illustrate more clearly the FS trend with doping. Also, as already mentioned, the introduced electron or hole charges in the modified VCA do not necessarily correspond to the
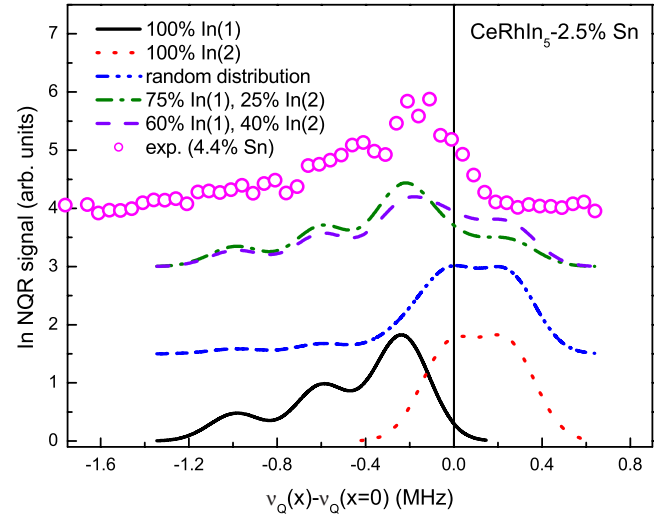

FIG. 5. (Color online) Computed doping dependence of the NQR resonances for 2.5% Sn in CeRhIn$_5$, using the LDA f-core approach. The Sn-doping atoms are assumed to replace In(1) and In(2) atoms, with probabilities as listed. Three of the curves have been shifted upward for visibility purpose. The measured NQR spectrum of CeRh(In$_{1-x}$Sn$_x$)$_5$, for $x=4.4\%$ Sn (symbols), is shown for comparison.

precise doping concentration, as a part of the introduced charges will be bound to the dopant atom. Moreover, in the lattice, there can locally exist a variation of introduced charges in the vicinity of a dopant atom. One substituted Cd atom per five In atoms would represent a situation with $x \approx 0.2$ locally. Hence, in the vicinity of the dopant atom antiferromagnetism could be favored through the above outlined mechanism, which would be consistent with recent experimental observations.[19]

2. Supercell calculations

The second approach to study the effect of doping on the NQR frequencies is computationally more demanding but also more accurate. We build $2 \times 2 \times 2$ supercells, in which one In atom is replaced by a dopant atom. Such supercell contains 40 In atoms, thus, replacing one means 2.5% doping. It is possible to replace an atom on either the In(1) or In(2) position. An important influence of the dopant atoms is that these reduce the symmetry of the system and thereby introduce a nonequivalency between the originally equivalent 8 In(1) atoms or 32 In(2) atoms, respectively. Depending on the relative position of the new equivalent groups of In atoms with respect to the dopant atom the quadrupolar frequency changes, which results in the experimentally observed splitting of the main resonance line. Furthermore, in this approach we can simulate a response corresponding to continuous mixtures of dopant atoms on In(1) and In(2) positions, i.e., ranging from all dopant atoms at the In(1) site to all at the In(2) site.

For CeRh(In$_{1-x}$Sn$_x$)$_5$, we have performed only f-core calculations, while for CeCo(In$_{1-x}$Cd$_x$)$_5$ we considered both the f-core and f-itinerant approaches. Figure 5 shows the computed NQR spectra for 2.5% Sn doping in CeRhIn$_5$.
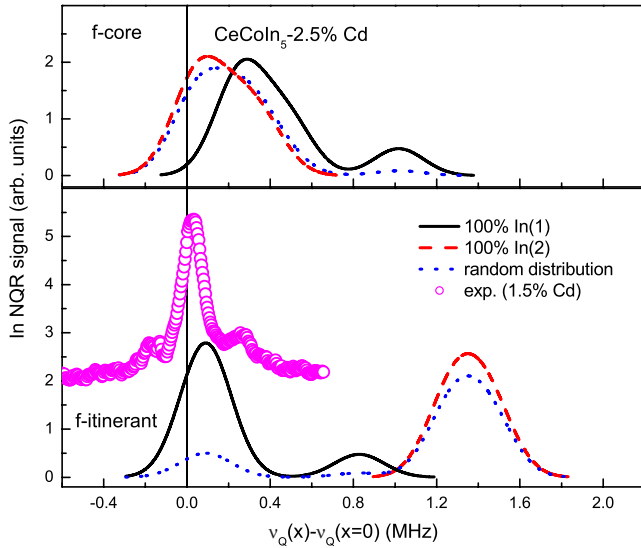
FIG. 6. (Color online) Computed doping dependence of the NQR resonances for 2.5% Cd substituted on In positions in CeCoIn$_5$. Top panel: LDA f-core calculation, bottom panel: LDA f-itinerant approach. Also shown is the experimental NQR spectrum of CeCo(In$_{1-x}$Cd$_x$)$_5$ for 1.5% Cd doping (symbols).

For comparison, the measured NQR spectrum of CeRh(In$_{1-x}$Sn$_x$)$_5$ for 4.4% Sn doping is also shown. A calculation with Sn only on the In(2) position leads to a side peak at a higher NQR frequency than the main line, which does not display a notable frequency change itself. Conversely, the assumption that all Sn doping goes in the In(1) position leads to a shift of the main line A to a lower frequency, as well as to the appearance of side peaks at lower frequencies. If we assume a completely random distribution of Sn, being with equal probabilities on In(1) and In(2) positions, the correspondence with the experimental NQR spectrum is poor (see Fig. 5). A good agreement with the measured NQR spectrum of CeRh(In$_{1-x}$Sn$_x$)$_5$ is obtained when we assume that the majority of Sn atoms goes in the In(1) positions and a smaller fraction goes in the In(2) positions. The experimental CeRh(In$_{1-x}$Sn$_x$)$_5$ NQR spectrum (see also Fig. 3) shows a shift of the main line to lower frequencies, a small shoulder on the high-frequency side of the main peak, and a broader side peak on the low-frequency side. These features are all present in the theoretical spectrum, assuming that the Sn atom goes for 60%–75% on an In(1) position and for 40%–25%, respectively, on an In(2) position. A recent extended x-ray absorption fine structure (EXAFS) investigation showed that the Sn atoms preferably substitute within the Ce-In plane with an estimated fraction of 60% substituting on an In(1) position.[17] This is in good agreement with the Sn distribution estimated from the calculated NQR spectra.

Our calculated results for 2.5% Cd doping in CeCoIn$_5$ are shown in Fig. 6. The NMR frequency shifts computed with the f-core and f-itinerant approaches have some distinct features. The experiment identifies the main line A and two side peaks, B and C (see experimental NQR spectrum for 1.5% Cd doping in Fig. 6). As mentioned above, it is likely that the peak C is due to an impurity phase since it shows a different T_N, as compared to the A and B peaks. Actually, in the cal-

culations, we never obtain the low-frequency side peak C, neither in the LDA f-core nor in the f-itinerant approach—which is consistent with the interpretation of peak C as an extrinsic experimental artifact. The other two effects of Cd doping in CeCoIn$_5$, the shift of the A line to higher frequencies and the appearance of a high-frequency B line, can be explained with both the f-core and f-itinerant models. The f-itinerant approach, assuming that all Cd occupies an In(1) position, qualitatively predicts the experimental NQR spectrum. The f-core calculation gives a similar trend but with a larger effect on the A line, which would not correspond well to the experimental observation. The spectral shape that matches best the experimental spectrum is in both cases obtained when it is assumed that the majority of the Cd atoms occupies the In(1) position.

C. Pressure dependence

It is straightforward to study computationally the change of the electric-field gradient with pressure. We performed a set of calculations, gradually reducing (or increasing) the lattice parameters while keeping the c/a ratio constant. These calculations were performed within the standard LDA; for CeRhIn$_5$, it was additionally done with the open-core approach. The calculations predict a nearly linear decrease in the EFG with increasing volume. The EFG at In(1) decreases by 0.64%, 0.66%, 0.72%, and 0.63% per 1% volume increase for CeCoIn$_5$, CeRhIn$_5$ (itinerant and localized), and CeIrIn$_5$, respectively. The decrease in EFG with increasing volume can be qualitatively understood as an effect of smoothening the charge distribution (i.e., reducing its derivatives) with increasing interatomic distance. Experimentally we find that $d\nu_Q[\text{In}(1)]/dP = 63(2)$ kHz/GPa in CeCo(In$_{0.9}$Cd$_{0.1}$)$_5$ and 53(5) kHz/GPa in CeRhIn$_5$. The bulk moduli of CeRhIn$_5$ and CeCoIn$_5$ are 85.4 and 76.1 GPa, respectively.[48] These values give decreases for the EFGs by 0.59% and 0.67% in CeCoIn$_5$ and CeRhIn$_5$, respectively, for a 1% volume increase. These numbers are very close to the predicted values.

V. ELECTRONIC STRUCTURES

The computed NQR frequencies depend on the approach adopted for the 4f electronic structure. For the discussion of which electronic structure model provides the best description of these materials, it is instructive to consider how the band structure evolves when the degree of f electron localization is gradually increased by increasing U from the f-itinerant approximation to the f-localized approximation.

In Fig. 7 we show the energy bands of CeCoIn$_5$, computed with the GGA+U approach for U=1, 3, and 6 eV, respectively, as well as the energy bands obtained with the f-core approach (bottom panel). The energy bands for the f-itinerant case (GGA) are not shown here as a similar LDA band structure has already been shown earlier.[37] The GGA +U bands obtained with U=1 eV are very close to those of the f-itinerant GGA approach (cf. Ref. 37). In Fig. 7 the f character of the bands is shown by the red color and fatness of the bands. The bands computed with U=1 eV display a
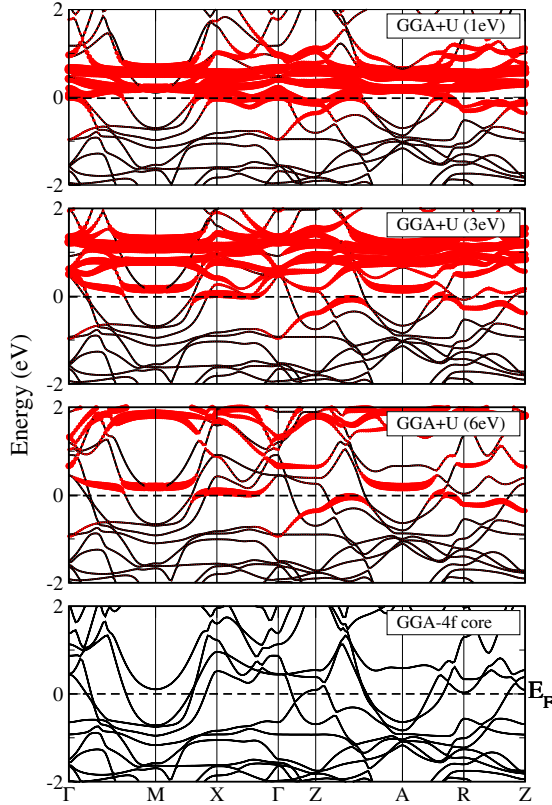
FIG. 7. (Color online) Energy bands of nonmagnetic CeCoIn$_5$, computed using the GGA+U and f-core approaches. GGA+U band dispersions are given for U=1, 3, and 6 eV, respectively. The amount of Ce f character in the bands is highlighted by the fatness of the bands plotted in red color. Note the flat 4f band contributions that persist near the Fermi energy with increasing Coulomb U value.

manifold of f bands straddling the Fermi level and dispersing up to 2 eV above E_F. With increasing value of the effective Coulomb U, the 4f manifold of bands starts to split and the upper Hubbard band becomes placed at higher energies; for an effective U of 6 eV, it is located somewhat above 2 eV. The lower 4f band appears just below or close to the Fermi level. An interesting yet unusual feature of this band is its energy position, which practically does not change with increasing the U value. For U=1 eV, for example, there is a flat 4f band below E_F at the R to Z high-symmetry direction, which remains at the same energy position when the U is increased to 3 and 6 eV. In the Γ-Z-A direction, there is a dispersive f band, which disperses from −1 eV at the Γ point to touching the Fermi level between Z and A; also, this f band part practically does not change its energy position with increasing f-localization degree by increasing U. Another f band part can be recognized between the X and Γ points, where a very flat f band lies on the Fermi level. This flat bands continues just above E_F along the Γ-M-X high-symmetry direction, again without modification in its self-consistently computed energy position even though the U is varied by several eV. We note that this pinned behavior of the lower 4f band is very different from what is commonly obtained for Ce compounds with relatively localized f electrons, where a Coulomb U of 6 eV places the 4f level at

about 3 eV below the Fermi level (see, e.g., Ref. 49). The GGA+U calculations predict consequently a high 4f density of states (DOS) close to E_F due to the pinning of the flat 4f state near the Fermi level. A similar behavior has previously been obtained with LDA+U calculations for the heavy-fermion material YbBiPt.[50] Since the flat 4f band in CeCoIn$_5$ consists of parts just below and above E_F, the 4f DOS at E_F exhibits a sharp double peak structure. The f contribution in the bands only disappears when the f-core approach is adopted (see bottom panel of Fig. 7). The very flat, occupied 4f band parts along the high-symmetry directions R-Z and X-Γ are now completely removed, as are also the flat unoccupied band parts near the A point and along the Γ-M direction. Such changes obviously lead to modifications of the Fermi surface; for example, near the R point and along the Γ-Z symmetry line.

Energy bands computed with the LDA+U or GGA+U method were not yet reported for the Ce-115 compounds. Recently, a LDA+U dynamical mean-field theory (LDA+U-DMFT) study of CeIrIn$_5$ was performed.[51] In the later study a U of 5 eV is used, a value which is close to the U=6 eV used in the present study. At variance with the present GGA+U calculations in Ref. 51, it is written that the LDA+U calculated lower and upper Hubbard bands are at −2.5 and 3 eV, respectively. Our GGA+U (U=6 eV) calculations predict conversely—for both CeCoIn$_5$ and CeIrIn$_5$ (not shown)—the lower 4f band to be very narrow and pinned near the Fermi level. In the GGA+U approach, with $U \approx 6$ eV, CeCoIn$_5$ would thus be classified as an intermediate-valence material. According to Ref. 51 the dynamical self-energy aspects of DMFT lead to a narrow 4f band at the Fermi level. Our GGA+U calculations predict a narrow 4f band at E_F but split with flat band parts slightly above and below E_F, which, moreover, is completely due to the static self-energy (see also Ref. 50 for similar behavior in YbBiPt). The origin of these differences are not understood and require further investigation.

VI. DISCUSSION AND CONCLUSIONS

A major question in Kondo lattice materials such as the Ce-115 compounds is how the crossover from f-localized behavior at high temperature to f-delocalized behavior at low temperatures takes place. A recent two-fluid analysis[40] of transport data of CeCoIn$_5$ predicts that a crossover from single-ion Kondo behavior, characterized by localized f electrons, to Kondo lattice behavior, characterized by the development of lattice coherence and delocalization of the f electrons, starts to happen below 45 K. At low temperatures (<500 mK), de Haas–van Alphen experiments on CeCoIn$_5$, in conjunction with *ab initio* calculations support a large degree of f delocalization.[36–38,47] In contrast, in CeRhIn$_5$, the f electron is localized even at low temperatures as follows from low-temperature de Haas–van Alphen and neutron-scattering experiments.[15,37,52,53] The situation for CeIrIn$_5$ is more complex. de Haas–van Alphen experiments, as well as angular-resolved photoemission (ARPES) experiments, indicate a reasonable degree of f-electron delocalization at low temperatures (<500 mK) [37,54] as well as at 10 K.[55]

Our calculated EFGs support clearly the picture of localized f states in CeRhIn$_5$. This finding is fully consistent with the physical picture that has been obtained from the recent de Haas–van Alphen investigations.[15,37] For CeCoIn$_5$, the measured NQR frequencies could be reasonably explained by a moderate $U \approx 3$ eV. This is particularly true for the In(1) NQR frequency. The In(2) NQR data seem to agree best for a localized f calculation. The $U \approx 3$ eV electronic structure nevertheless appears to be preferable, first, because the In(1) atom is surrounded by four Ce atoms and, thus, expected to be more sensitive to the f electronic structure. Second, a moderate Coulomb U of about 3 eV provides an electronic structure, which does not deviate very much from the f itinerant one. The latter electronic structure gives unambiguously a better explanation of the de Haas–van Alphen data measured below 500 mK than does the f-localized model.[36] The present NQR measurements have been performed at 4–5 K, which is a low temperature; nevertheless, a moderate change in the f-electron behavior toward localization is already conceivable. Resistivity measurements[56] show a clear change in the temperature-dependent resistivity occurring at about 4–5 K; a further temperature reduction of only 2 K induces the transition to the superconducting state at 2.3 K. Therefore, it is reasonable to expect that a small temperature difference of 4 K in this critical region could already have an effect on the electronic structure, which would reconcile the current findings with those from the low-temperature de Haas–van Alphen investigations. For CeIrIn$_5$, we observe that a larger U than 3 eV is needed in order to obtain satisfactory agreement with the experimental NQR frequencies. A Coulomb U of 6 eV is getting close to provide good agreement for the In(1) NQR frequency. The current results for the In(2) atom would again advocate f-electron localization in CeIrIn$_5$. Also for this material, de Haas–van Alphen experiments indicated a reasonable f-electron delocalization below 500 mK.[36,54] Recent ARPES experiments[55] indicated the development of a small, itinerant f-electron component along the Γ-X high-symmetry direction at 10 K. The GGA+U calculated energy bands for U=3–6 eV do indeed predict a narrow $4f$ band close E_F (cf. Fig. 7 for CeCoIn$_5$). LDA+U-DMFT calculations[51] predict a gradual f-electron delocalization in CeIrIn$_5$ below 50 K together with the development of a narrow itinerant f-electron component. Our observations concerning the increased Coulomb U for CeIrIn$_5$ are consistent with the trend in the CeCoIn$_5$ and CeIrIn$_5$ materials, where the latter is believed to be the somewhat more localized $4f$ material. Further investigations appear to be needed to understand why LDA+U-DMFT predicts a lower Hubbard $4f$ band at −2.5 eV.

Our investigations of the NQR of doped Ce-115 materials confirm that the f-core approach provides a good explanation for Sn-doped CeRhIn$_5$. The Cd-doped CeCoIn$_5$, neither with the f-itinerant nor with the f-localized approach, agree well with the measured NQR spectra. Nevertheless, the calculations performed for doped Ce-115 materials shed light, in addition, on the origin of the various peaks in the measured NQR spectra. The shift of the main NQR line in Sn-doped CeRhIn$_5$ and the occurrence of side peaks are well explained by the supercell calculations. The frequency shift of the main NQR line and shape of the NQR spectrum of doped CeCoIn$_5$ are reasonably explained by f-itinerant calculations. For both doped Ce-115 materials, the NQR side peaks arise from the symmetry-breaking effect of the impurity atom, i.e., the side peaks are In(1) that are nearest neighbors to the dopants. Our calculations indicate that for both CeCoIn$_5$ and CeRhIn$_5$, the dopant atom substitutes preferably on the In(1) position, in agreement with experimental observations.[17] Furthermore, our results indicate that Sn/Cd doping in the Ce-115's can be modeled by a corresponding, effective electron/hole doping. The changes in carrier concentration lead to significant changes in the Fermi-surface topology, which are likely connected to the dramatic changes in the ground state appearing in these systems. Whether the change of the Fermi surface is the sole origin of the ground-state changes or not remains an open question.

To conclude, we have investigated theoretically and experimentally the NQR frequencies of pure, as well as doped, Ce-115 compounds. A particular aim of our study is to establish, as well as develop, the NQR technique as a probe of the electronic structure. Indeed our results confirm that, in combination with DFT-based calculations, NQR offers a new window of the f electronic structure.

---

*jan.rusz@fysik.uu.se

[1] C. P. Slichter, *Principles of Magnetic Resonance*, 3rd ed. (Springer-Verlag, New York, 1990).

[2] N. J. Curro, T. Caldwell, E. D. Bauer, L. A. Morales, M. J. Graf, Y. Bang, A. V. Balatsky, J. D. Thompson, and J. L. Sarrao, Nature (London) **434**, 622 (2005).

[3] I. Farnan, H. Cho, and W. J. Weber, Nature (London) **445**, 190 (2007).

[4] G.-q. Zheng, K. Tanabe, T. Mito, S. Kawasaki, Y. Kitaoka, D. Aoki, Y. Haga, and Y. Ōnuki, Phys. Rev. Lett. **86**, 4664 (2001).

[5] R. Movshovich, M. Jaime, J. D. Thompson, C. Petrovic, Z. Fisk, P. G. Pagliuso, and J. L. Sarrao, Phys. Rev. Lett. **86**, 5152 (2001).

[6] P. G. Pagliuso, C. Petrovic, R. Movshovich, D. Hall, M. F. Hundley, J. L. Sarrao, J. D. Thompson, and Z. Fisk, Phys. Rev. B **64**, 100503(R) (2001).

[7] V. S. Zapf, E. J. Freeman, E. D. Bauer, J. Petricka, C. Sirvent, N. A. Frederick, R. P. Dickey, and M. B. Maple, Phys. Rev. B **65**,

014506 (2001).

[8] R. J. Ormeno, A. Sibley, C. E. Gough, S. Sebastian, and I. R. Fisher, Phys. Rev. Lett. **88**, 047005 (2002).

[9] T. Park, F. Ronning, H. Q. Yuan, M. B. Salamon, R. Movshovich, J. L. Sarrao, and J. D. Thompson, Nature (London) **440**, 65 (2006).

[10] C. Petrovic, R. Movshovich, M. Jaime, P. G. Pagliuso, M. F. Hundley, J. L. Sarrao, Z. Fisk, and J. D. Thompson, Europhys. Lett. **53**, 354 (2001).

[11] W. Bao, P. G. Pagliuso, J. L. Sarrao, J. D. Thompson, Z. Fisk, J. W. Lynn, and R. W. Erwin, Phys. Rev. B **62**, R14621 (2000).

[12] N. J. Curro, P. C. Hammel, P. G. Pagliuso, J. L. Sarrao, J. D. Thompson, and Z. Fisk, Phys. Rev. B **62**, R6100 (2000).

[13] H. Hegger, C. Petrovic, E. G. Moshopoulou, M. F. Hundley, J. L. Sarrao, Z. Fisk, and J. D. Thompson, Phys. Rev. Lett. **84**, 4986 (2000).

[14] H. Shishido, R. Settai, S. Araki, T. Ueda, Y. Inada, T. C. Kobayashi, T. Muramatsu, Y. Haga, and Y. Ōnuki, Phys. Rev. B **66**, 214510 (2002).

[15] H. Shishido, R. Settai, H. Harima, and Y. Ōnuki, J. Phys. Soc. Jpn. **74**, 1103 (2005).

[16] L. D. Pham, T. Park, S. Maquilon, J. D. Thompson, and Z. Fisk, Phys. Rev. Lett. **97**, 056404 (2006).

[17] M. Daniel, E. D. Bauer, S.-W. Han, C. H. Booth, A. L. Cornelius, P. G. Pagliuso, and J. L. Sarrao, Phys. Rev. Lett. **95**, 016406 (2005).

[18] J. Paglione, T. A. Sayles, P.-C. Ho, J. R. Jeffries, and M. B. Maple, Nat. Phys. **3**, 703 (2007).

[19] R. R. Urbano, B.-L. Young, N. J. Curro, J. D. Thompson, L. D. Pham, and Z. Fisk, Phys. Rev. Lett. **99**, 146402 (2007).

[20] M. T. Czyzyk and G. A. Sawatzky, Phys. Rev. B **49**, 14211 (1994).

[21] V. I. Anisimov, I. V. Solovyev, M. A. Korotin, M. T. Czyzyk, and G. A. Sawatzky, Phys. Rev. B **48**, 16929 (1993).

[22] A. Bianchi, R. Movshovich, I. Vekhter, P. G. Pagliuso, and J. L. Sarrao, Phys. Rev. Lett. **91**, 257001 (2003).

[23] P. Blaha, K. Schwarz, G. K. H. Madsen, D. Kvasnicka, and J. Luitz, *WIEN2k, An Augmented Plane Wave + Local Orbitals Program for Calculating Crystal Properties* (Karlheinz Schwarz, Techn. Universität Wien, Austria, 2001).

[24] J. Kuneš, P. Novák, M. Divis, and P. M. Oppeneer, Phys. Rev. B **63**, 205111 (2001).

[25] P. Blaha, K. Schwarz, and P. Herzig, Phys. Rev. Lett. **54**, 1192 (1985).

[26] P. Herzig, Theor. Chim. Acta **67**, 323 (1985).

[27] P. Mohn, Hyperfine Interact. **128**, 67 (2000).

[28] C. Petrovic, P. G. Pagliuso, M. F. Hundley, R. Movshovich, J. L. Sarrao, J. D. Thompson, Z. Fisk, and P. Monthoux, J. Phys.: Condens. Matter **13**, L337 (2001).

[29] J. P. Perdew and Y. Wang, Phys. Rev. B **45**, 13244 (1992).

[30] J. P. Perdew, K. Burke, and M. Ernzerhof, Phys. Rev. Lett. **77**, 3865 (1996).

[31] Y. Kohori, Y. Inoue, T. Kohara, G. Tomka, and P. C. Riedi, Physica B **259&261**, 103 (1999).

[32] J. Rusz and M. Biasini, Phys. Rev. B **71**, 233103 (2005).

[33] Y. Kohori, Y. Yamato, Y. Iwamoto, T. Kohara, E. D. Bauer, M. B. Maple, and J. L. Sarrao, Phys. Rev. B **64**, 134526 (2001).

[34] N. J. Curro, B. Simovic, P. C. Hammel, P. G. Pagliuso, J. L. Sarrao, J. D. Thompson, and G. B. Martins, Phys. Rev. B **64**, 180514(R) (2001).

[35] D. W. Lynch and J. H. Weaver, in *Handbook on the Physics and Chemistry of Rare Earths*, edited by K. A. Gschneidner, L. Eyring, and S. Hüfner (North-Holland, Amsterdam, 1987), Vol. 10, p. 231.

[36] H. Shishido, R. Settai, D. Aoki, S. Ikeda, H. Nakawaki, N. Nakamura, T. Iizuka, Y. Inada, K. Sugiyama, T. Takeuchi, K. Kindo, T. C. Kobayasi, Y. Haga, H. Harima, Y. Aoki, T. Namiki, H. Sato, and Y. Ōnuki, J. Phys. Soc. Jpn. **71**, 162 (2002).

[37] S. Elgazzar, I. Opahle, R. Hayn, and P. M. Oppeneer, Phys. Rev. B **69**, 214510 (2004).

[38] P. M. Oppeneer, S. Elgazzar, A. B. Shick, I. Opahle, J. Rusz, and R. Hayn, J. Magn. Magn. Mater. **310**, 1684 (2007).

[39] E. D. Bauer, C. Capan, F. Ronning, R. Movshovich, J. D. Thompson, and J. L. Sarrao, Phys. Rev. Lett. **94**, 047001 (2005).

[40] S. Nakatsuji, D. Pines, and Z. Fisk, Phys. Rev. Lett. **92**, 016401 (2004).

[41] N. J. Curro, B.-L. Young, J. Schmalian, and D. Pines, Phys. Rev. B **70**, 235117 (2004).

[42] M. Yashima, S. Kawasaki, Y. Kawasaki, G.-q. Zheng, Y. Kitaoka, H. Shishido, R. Settai, Y. Haga, and Y. Ōnuki, J. Phys. Soc. Jpn. **73**, 2073 (2004).

[43] S. Kawasaki, G.-q. Zheng, H. Kan, Y. Kitaoka, H. Shishido, and Y. Ōnuki, Phys. Rev. Lett. **94**, 037007 (2005).

[44] J. Haase, O. P. Sushkov, P. Horsch, and G. V. M. Williams, Phys. Rev. B **69**, 094504 (2004).

[45] N. J. Curro *et al.* (unpublished).

[46] M. Nicklas, O. Stockert, T. Park, K. Habicht, K. Kiefer, L. D. Pham, J. D. Thompson, Z. Fisk, and F. Steglich, Phys. Rev. B **76**, 052401 (2007).

[47] R. Settai, H. Shishido, S. Ikeda, Y. Murakawa, M. Nakashima, D. Aoki, Y. Haga, H. Harima, and Y. Ōnuki, J. Phys.: Condens. Matter **13**, L627 (2001).

[48] P. S. Normile, S. Heathman, M. Idiri, P. Boulet, J. Rebizant, F. Wastin, G. H. Lander, T. Le Bihan, and A. Lindbaum, Phys. Rev. B **72**, 184508 (2005).

[49] P. M. Oppeneer, in *Handbook of Magnetic Materials*, edited by K. H. J. Buschow (Elsevier, Amsterdam, 2001), Vol. 13, pp. 229–422.

[50] P. M. Oppeneer, V. N. Antonov, A. N. Yaresko, A. Y. Perlov, and H. Eschrig, Phys. Rev. Lett. **78**, 4079 (1997).

[51] J. H. Shim, K. Haule, and G. Kotliar, Science **318**, 1615 (2007).

[52] U. Alver, R. G. Goodrich, N. Harrison, D. W. Hall, E. C. Palm, T. P. Murphy, S. W. Tozer, P. G. Pagliuso, N. O. Moreno, J. L. Sarrao, and Z. Fisk, Phys. Rev. B **64**, 180402(R) (2001).

[53] A. D. Christianson, J. M. Lawrence, P. G. Pagliuso, N. O. Moreno, J. L. Sarrao, J. D. Thompson, P. S. Riseborough, S. Kern, E. A. Goremychkin, and A. H. Lacerda, Phys. Rev. B **66**, 193102 (2002).

[54] Y. Haga, Y. Inada, H. Harima, K. Oikawa, M. Murakawa, H. Nakawaki, Y. Tokiwa, D. Aoki, H. Shishido, S. Ikeda, N. Watanabe, and Y. Ōnuki, Phys. Rev. B **63**, 060503(R) (2001).

[55] S.-I. Fujimori, A. Fujimori, K. Shimada, T. Narimura, K. Kobayashi, H. Namatame, M. Taniguchi, H. Harima, H. Shishido, S. Ikeda, D. Aoki, Y. Tokiwa, Y. Haga, and Y. Ōnuki, Phys. Rev. B **73**, 224517 (2006).

[56] J. Paglione, M. A. Tanatar, D. G. Hawthorn, F. Ronning, R. W. Hill, M. Sutherland, L. Taillefer, and C. Petrovic, Phys. Rev. Lett. **97**, 106606 (2006).